Published in final edited form as:
Dev Neurobiol. 2008 May ; 68(6): 760–770. doi:10.1002/dneu.20621.

In Vivo Imaging of Presynaptic Terminals and Postsynaptic Sites in the Mouse Submandibular Ganglion

Corey M. McCann and **Jeff W. Lichtman**
Department of Molecular and Cellular Biology, Harvard University, Cambridge, Massachusetts 02138

Abstract

Much of what is currently known about the behavior of synapses *in vivo* has been learned at the mammalian neuromuscular junction, because it is large and accessible and also its postsynaptic acetylcholine receptors (AChRs) are readily labeled with a specific, high-affinity probe, α-bungarotoxin (BTX). Neuron–neuron synapses have thus far been much less accessible. We therefore developed techniques for imaging interneuronal synapses in an accessible ganglion in the peripheral nervous system. In the submandibular ganglion, individual preganglionic axons establish large numbers of axo-somatic synapses with postganglionic neurons. To visualize these sites of synaptic contact, presynaptic axons were imaged by using transgenic mice that express fluorescent protein in preganglionic neurons. The postsynaptic sites were visualized by labeling the acetylcholine receptor (AChR) α7 subunit with fluorescently tagged BTX. We developed *in vivo* methods to acquire three-dimensional image stacks of the axons and postsynaptic sites and then follow them over time. The submandibular ganglion is an ideal site to study the formation, elimination, and maintenance of synaptic connections between neurons *in vivo*.

Keywords

timelapse; bungarotoxin; synapse; *in vivo*; submandibular

Introduction

The fine details of the formation, maintenance, and elimination of synaptic connections between neurons remain largely unknown. We lack knowledge about these processes, in part, because it is difficult to directly observe synapses in intact living brains due to several practical problems. First, the skull, spinal vertebrae, and meninges surround the brain and spinal cord and limit the introduction of electrodes, imaging objectives, and chemical reagents into the central nervous system (CNS). Second, CNS neurons typically have elaborate dendritic trees that are distributed over a large volume of neuropil, making it difficult to image the dendritic arbor within a single, well-resolved optical field, and thus to identify the cells of origin at most postsynaptic sites. Third, further complicating matters, CNS neurons receive synaptic input from diverse neuronal subtypes. Lastly, simultaneous marking of presynaptic terminals and postsynaptic structures, desirable for understanding the wiring of CNS circuits, has thus far been technically challenging in the CNS.

The neuromuscular junction (NMJ) provides a useful paradigm for what an *in vivo* synaptic preparation should be. This synapse is useful for *in vivo* synaptic studies because of its optical

Correspondence to: J.W. Lichtman (jeff@mcb.harvard.edu).

accessibility, simple organization, and ease of labeling (Sanes and Lichtman, 2001). For example, by making an incision in the neck, synaptic inputs to superficial muscles can be easily accessed and repeatedly imaged for months in living animals (Lichtman et al., 1987). Since all of the synapses onto an individual muscle fiber are colocalized to the same small endplate region, it is possible to identify all the axonal inputs to a multiply innervated postsynaptic muscle cell during development (Walsh and Lichtman, 2003). In adults, only a single axon innervates each endplate, making unambiguous identification of the site and source of input straightforward over many imaging sessions. The low density of motor axons innervating muscle fibers also allows for the tracing of large portions of single motor axon branching patterns *in vivo* (Nguyen et al., 2002). All the advantages of the neuromuscular system have recently been amplified by advances in transgenic technology, which permit multicolor labeling of motor axons and their synaptic terminals based on expression of spectral variants of the Green Fluorescent Protein (Feng et al., 2000). The NMJ also has a unique advantage in that its postsynaptic sites can be labeled *in vivo* with fluorescent conjugates of α-bungarotoxin (BTX), a snake venom toxin that binds to acetylcholine receptors (AChRs) with high affinity and specificity (Lee et al., 1967). This postsynaptic labeling allows clear identification of the location of presynaptic terminals. In addition, because BTX is readily derivatized to produce different kinds of conjugates, this toxin has many different applications. For example, pioneering studies on synaptic structure and function have relied on agarose-conjugated BTX to purify AChRs (Changeux et al., 1971), ^{125}I-BTX to count AChRs (Fertuck and Salpeter, 1976), and fluorescent BTX to track and visualize AChRs (Anderson and Cohen, 1977). In fact, BTX has been such an effective marker for labeling cell-surface receptors, that several groups have fused BTX-binding domains to ectodomains of transmembrane proteins and used BTX conjugates to label and purify the tagged molecules (Sekine-Aizawa and Huganir, 2004; McCann et al., 2005). By combining genetic with pharmacological fluorescent labeling methods, it is possible to assess dynamically at high temporal and spatial resolution interactions between multiple synaptic elements in ways that would be hard to imagine using other approaches.

Our goal here was to develop a preparation, with the same kind of experimental advantages found in the neuromuscular system, to allow comparable studies of synaptic connections between neurons. In this report, we undertake high-resolution imaging of the pre- and postsynaptic elements of synapses in the submandibular ganglion (SMG), an accessible part of the parasympathetic nervous system where time-lapse imaging is technically feasible (Purves and Lichtman, 1987; Gan et al., 2003). To visualize these connections, pre- and postganglionic neurons were labeled with fluorescent proteins. We show that BTX can be used to label SMG synapses, that this labeling corresponds to postsynaptic AChRs containing the α7 subunit and that this label can be used to visualize postsynaptic neurotransmitter receptors over time in living animals. Because it is possible to obtain high-resolution confocal stacks at multiple time points of both presynaptic axons and their postsynaptic sites, the SMG may be an ideal interneuronal preparation to study the details of synaptic maturation, maintenance, and aging.

Materials and Methods

Labeling SMG Neurons with Fluorescent Proteins

New thy1 transgenic lines were created as reported previously (Feng et al., 2000). Founder animals were bred to CD-1 mice and the progeny screened for preganglionic or postganglionic SMG expression. For some experiments, transgenic lines exhibiting a desirable SMG expression pattern (such as subset expression of preganglionic axons with YFP) were crossed to thy1 animals expressing contrasting fluorescent proteins in other neurons (i.e., CFP in all preganglionic axons or in some postganglionic neurons).

To analyze the labeling, we dissected the SMG after intracardial perfusion with 4% paraformaldehyde (PFA) in phosphate buffered saline (PBS, pH 7.4). SMGs were post-fixed for 30 min in 4% PFA in PBS and the surrounding tissue was removed to leave the salivary ducts. Salivary ducts were mounted in Vectashield (Vector Laboratories, Burlingame, CA) underneath a coverslip and imaged with a laser scanning confocal microscope (Olympus FV 1000, Melville, NY) with either an Olympus Plan Apo 40× oil (1.3 NA) or 603× oil (1.45 NA) objective. All multicolor images were acquired sequentially to avoid fluorescent bleed-through. Z-stacks were flattened and γ-values manipulated using Metamorph Software (Universal Imaging, Downing-town, PA) to provide acceptable contrast.

Labeling Postganglionic AChRs with α-Bungarotoxin

All BTX labeling was done *in vivo*. Animals were anesthetized and mechanically ventilated as reported previously (Gan et al., 2003). Following a ventral midline incision in the neck, submandibular ganglia were exposed (Purves and Lichtman, 1987) and bathed in lactated Ringer's solution (Baxter, Deerfield, IL) containing 5 μmL rhodamine-conjugated BTX (TRITC-BTX) or Alexa647-conjugated BTX (647-BTX) (Molecular Probes, Eugene, OR). To allow for full penetration through the connective tissue capsule surrounding each ganglion, the BTX solution was kept in the neck for 1–2 h. Unbound BTX was removed by a 10–30-min wash with a continuous perfusion of Ringer's solution. In some cases BTX-treated animals were fixed and dissected and SMGs were mounted onto slides and imaged as earlier.

Blockade of BTX Binding

Animals were anesthetized, intubated, and the SMGs exposed. For preblocking, the ganglion was bathed for 30 min in Ringer's solution containing a cholinergic antagonist (10 μM unlabeled BTX or 10 n*M* methyllycaconitine, MLA). 5 n*M* TRITC-BTX was then added to the preblocking solution and allowed to remain in the neck for 1 h. Control labeling was conducted by omitting unlabeled BTX and MLA, and adding TRITC-BTX. SMGs were then washed with Ringer's solution, fixed with PFA and mounted for imaging. Imaging parameters (i.e., PMT voltage, gain, offset, zoom, pixel number, bit depth, and scan speed) were set to acquire a full dynamic range of intensities from the BTX-labeled sites of control ganglia. Ganglia from all treatments were then imaged using the same microscope settings.

In Vivo Imaging

Animals were anesthetized and intubated as described previously (Gan et al., 2003). SMGs were exposed and AChRs were labeled with 647-BTX as described earlier. A small polished metal platform was placed under the salivary ducts to elevate the SMG. Another metal probe was placed over the submandibular and sublingual glands to stabilize the ganglia. BTX-labeled AChRs were identified using a CCD camera (Retiga SRV, QImaging, Burnaby, BC, Canada) and then image stacks were taken on a laser scanning microscope (Zeiss 510 Meta, Thornwood, NY) using confocal or 2-photon microscopy (Spectra-physics, Mountain View, CA) with either an Olympus 60× water immersion (1.1 NA) or Zeiss 63× water immersion (1.0 NA) objective. To image preganglionic axons and BTX-labeled AChRs, both channels were acquired simultaneously using the 488 and 633 nm lines of the confocal microscope. Image stacks were sampled at or beyond the Nyquist limit in XY. XY images in a stack were obtained at 0.5-μm steps. Z-stacks were flattened and γ-values manipulated using Metamorph Software. Processing was performed identically for all planes of a Z-stack.

For single-session time-lapse imaging, the microscope was covered with a nylon curtain and the temperature at the microscope stage was maintained at 34°C using an Air-Therm heater controller (World Precision Instruments, Sarasota, Fl). The neck was continuously perfused with warmed Ringer's solution, and anesthesia was maintained by administering ketamine and xylazine in half the induction dose approximately every 2 h.

For multiple session imaging, the animal was prepared and imaged as earlier. After acquiring image stacks, the neck was sutured closed and the animal returned to its cage. Additional images were acquired by repeating the procedures described earlier.

Nerve Crush

In anesthetized animals, salivary ducts were exposed and preganglionic axons were crushed by manually compressing the portion of the salivary duct between the submandibular gland and the digastric muscle. The neck was sutured closed and the animal was returned to the cage for recovery.

Results

Vital Labeling in the SMG

Two types of neurons exist in the rodent SMG (Lichtman, 1977; Snider, 1987). Preganglionic neurons, whose cell bodies lie in the superior salivatory nucleus of the brain stem, project axons to the ganglion via the lingual nerve. These axons then project along the salivary ducts [Fig. 1 (A), green axons] where they encounter ganglion cell clusters and form cholinergic synapses. The ganglion cells or postganglionic neurons are arranged in scattered small- to moderate-sized clusters (5–500 cells). They project postganglionic axons that enter the sublingual and larger submandibular salivary glands where they innervate gland parenchymal cells [Fig. 1(A), blue axons].

We screened transgenic mice in which the thy1 promoter drives the expression of fluorescent proteins (Feng et al., 2000) and also generated new thy1 XFP lines to identify lines labeling pre- and/or postganglionic cells in the submandibular ganglion. We found some lines that express fluorescent proteins brightly in subsets of preganglionic neurons but are not expressed in postganglionic neurons [Fig. 1(B_1,C)]. Other lines had fluorescent protein expression primarily in postganglionic neurons leaving preganglionic axons unlabeled [Fig. 1(B_2)]. Lines expressing spectrally distinct fluorophores were crossed to produce animals with multiple color preganglionic axons [Fig. 1(C)] or with contrasting pre- and postsynaptic neurons [Fig. 1(B)]. These crosses show that each ganglion cell typically receives a basket-like ensemble of synapses from an individual preganglionic axon. The postganglionic labeling shows that most adult cells have very fine and extremely short processes (<1 μm) extending from the soma and axon initial segment [Fig. 1(B_3)]. The sites of these processes coincide with the regions where preganglionic axons make synaptic contact. This juxtaposition suggests that synapses are not axo-somatic *per se*, but rather localize to fine pseudodendrites. Ultrastructural analysis of the submandibular ganglion in rodents confirms this impression (Lichtman, 1977).

Nonneuronal cells associated with the submandibular ganglion can also be labeled using transgenic approaches. Figure 1(D) shows labeled Schwann cells associated with ganglion cells in a mouse line where the S100 promoter drives the expression of GFP (Zuo et al., 2004). Two to three Schwann cells envelop each postganglionic neuron. This layer encircles both the soma and all the synaptic contacts.

BTX Labeling AChRs in the SMG

The 74-amino acid polypeptide snake toxin, BTX has been an ideal marker of the postsynaptic membrane at the NMJ because of its strong binding to, and high degree of specificity for, muscle type AChRs (Lee et al., 1967). Since BTX is known to bind to a subset of neuronal nicotinic AChRs (Colquhoun and Patrick, 1997), we attempted to label the cholinergic synapses in the living SMG using a fluorescently tagged conjugate of this toxin.

Fluorescently tagged BTX did label the surfaces of postgangloinc neurons in the SMG. We labeled the SMG with BTX using a method similar to the one used at the NMJ. To label neuromuscular synapses *in vivo*, BTX is added to the bath solution surrounding a superficial muscle in an anesthetized animal through an incision in the skin (Balice-Gordon and Lichtman, 1990). To label SMG cells, the animal was first anesthetized with a mixture of ketamine and xylazine before the hair was removed from the ventral portion of the neck with a chemical depilatory. Following a ventral midline incision in the neck, the superficial fascia was blunt dissected from the salivary gland. Retractors were used to separate the superficial fascia away from the midline, creating a cavity in the neck into which fluids could be introduced. Next, using a pair of blunt-tipped forceps, the connective tissue surrounding the salivary ducts was removed to expose the ganglia affixed to the ducts. A mixture of Ringer's solution and fluorescent BTX (5 μg/mL) was added to the neck cavity and the volume was maintained for 1–2 h by adding aliquots of the BTX solution. To remove background fluorescence, the neck cavity was washed with a constant perfusion of pure Ringer's solution for 15 min before imaging.

Initially, to assay for BTX staining, we paraformaldehyde-fixed the previously labeled SMG by intracardial perfusion and then excised the ganglia and mounted them on a slide. At low magnification, postganglionic neurons appeared to be outlined with bright fluorescence [Fig. 2(A)]. Inspection at higher magnification revealed fluorescent puncta on the cell surface [Fig. 2(A), inset]. This labeling was specific as follows: it was not visible in animals that had not been exposed to BTX (data not shown) and it could be blocked by preincubation with a saturating amount of unlabeled BTX [Fig. 2(B)].

In addition to the α1 AChR subunit found on the postsynaptic muscle membrane, BTX also binds to neuronal nicotinic AChRs containing the α7–α10 subunit (Colquhoun and Patrick, 1997) and to a subset of β3 subunit containing GABA receptors (McCann et al., 2006). Of these receptor subunit proteins, only AChR α7 is thought to be expressed in peripheral ganglia (Gotti and Clementi, 2004). To check whether the BTX labeling in the SMG was bound to AChR α7, we attempted to block BTX labeling with methyllycaconitine (MLA), a reagent that selectively blocks BTX binding to AChR α7 (Ward et al., 1990). When the SMG was preincubated with MLA, or when MLA was added to the fluorescent BTX solution, BTX labeling was no longer observed [Fig. 2(C)]. Consistent with this observation, when we attempted to label SMGs with BTX in AChR α7 null animals (Orr-Urtreger et al., 1997), no staining was observed [Fig. 2(D)]. These results imply that BTX specifically binds to AChR α7 in the mouse SMG.

Colabeling preganglionic axons suggested that BTX-labeled puncta were postsynaptic sites. When we added BTX to the SMG of transgenic animals with YFP-labeled preganglionic axons, we observed that BTX-labeled puncta were selectively located in the vicinity of presynaptic axons [Fig. 2(E)]. A closer inspection showed that presynaptic terminals and BTX-labeled AChRs were tightly interdigitated [Fig. 2(E_3)]. This complementary staining pattern would be expected for presynaptic terminals abutting postsynaptic pseudodentrites covered with AChRs.

To exclude the possibility that the fluorescent BTX was binding to presynaptic axons (Zarei et al., 1999), we attempted to label ganglia in which preganglionic axons had been removed via a previous nerve crush. At 12 h after the crush, we found that fluorescently labeled preganglionic axons were no longer present; however, BTX labeling was still punctate and unchanged in intensity. These results indicate that the BTX labeling was not originating from presynaptic sites.

Time-Lapse Imaging of SMG Synapses

We developed a method to image SMG synapses *in vivo* with both high spatial and temporal resolution. We anesthetized and mechanically ventilated animals as described previously (see Materials and Methods section). A ventral midline incision in the neck exposed the salivary glands. Using a pair of blunt forceps, we removed the connective tissue surrounding the salivary ducts on the right or left side to expose the SMG. To provide stability, an oblong-polished metal platform was placed underneath the ducts [Fig. 3(B), green arrow]. A second probe was placed on top of the salivary glands to provide additional stability [Fig. 3(B), red arrow]. The resulting preparation allowed optical access to a several hundred micron portion of the salivary ducts [Fig. 3(B), dashed white circle]. In that region typically several ganglion cell clusters could be imaged using a water immersion objective in an upright epi-fluorescence or laser scanning microscope [Fig. 3(A), white arrow].

By manipulating the position of the metal platforms that support the salivary ducts, we were able to minimize movement of the SMG without reducing blood flow through the capillaries to the ganglion cell clusters that were to be imaged. This stabilization also permitted imaging of SMG synapses while mechanically ventilating the animal. Since the ventilator remained on during imaging, we could use slow laser scanning to obtain diffraction-limited three-dimensional image stacks (1024 × 1024 pixels per image at 1 image per second for up to 200 images). Using this technique we could acquire data sets like the one shown in Figure 3(C), showing a 3D stereo-pair of the fluorescent preganglionic innervation to two adjacent postganglionic neurons. By allowing animals to recover after an imaging session, we were able to reexamine the same region on subsequent days or weeks and follow the same synaptic and cellular structures for many hours or days [Figs. 3(D) and 5(A–E)]. Such imaging showed that axonal branches are for the most part stable but occasionally branches show signs of growth, retraction, or change in caliber.

To watch SMG synapses with even higher temporal resolution (minutes to hours), we also developed a technique to continuously monitor the SMG. Instead of closing the neck in between images, the animal remained deeply anesthetized on the microscope stage throughout the course of imaging. This was accomplished by constant dosage of ketamine/xylazine using a syringe pump connected to a butterfly needle. To mimic physiological conditions, ambient temperature was maintained using a temperature-regulated blower and the pH of the solution surrounding the ganglion was maintained by the constant perfusion of the neck with Ringer's solution. Using this setup we were able to image the same synapses for hours without any signs of damage [Fig. 3(E)] and in the best cases, could maintain the animal for up to 40 h. Higher temporal resolution was also possible. Figure 3(F) shows a small group of presynaptic boutons imaged every minute for 35 min.

Time-Lapse Imaging of Preganglionic Axon Growth and Synapse Formation

We caused degeneration by forceps crushing the preganglionic axons on the salivary ducts at a site that is proximal to the location of most ganglion cell clusters. Several days after the nerve crush surgery, we observed many blind-ending preganglionic axons projecting toward postganglionic neurons. To determine whether these axons were retracting or growing, we imaged them for several hours using our single-session time-lapse imaging protocol (described earlier). Over periods of minutes to hours, axonal processes could be seen to grow, often by extending at their tips in a highly dynamic way [Fig. 4(A)]. Rates of axonal growth often reached 20 μm/h. When the regrowing axons approached postganglionic neurons, they extended a branch that grew along the perimeter of the soma. The axon then wrapped around the postganglionic neuron by adding additional branches, most of which were initiated as collaterals proximal to the axon terminus [Fig. 4(B)]. As these preganglionic branches were elaborated they changed from uniform caliber to a more scalloped appearance over several

hours, and then remained stable for longer periods suggesting that these processes were presynaptic [Fig. 4(C)].

Time-Lapse Imaging of Pre- and Postsynaptic Structures

As shown earlier, by applying fluorescent BTX to the saline solution bathing the necks of living mice, we were able to label postsynaptic AChRs at SMG synapses. We were interested to know whether we could also use BTX to repeatedly image postsynaptic sites in living animals. AChRs were labeled using a near-infrared fluorescent conjugate of BTX and then confocal image stacks were obtained as described earlier [Fig. 5(A_1)]. After the imaging session, the dermis was sutured and animals were allowed to recover. At 1 or more subsequent time points separated by 5–50 h, the animal was reanesthetized and surface AChRs were revisualized by reapplying fluorescent BTX. Using this technique, we could image the same ganglion cell's AChRs over periods of days [Fig. 5(A–E)].

The distribution of postsynaptic AChRs as labeled by BTX remained stable over the intervals studied here [Fig. 5(A–E), red channel]. Most of the presynaptic terminals associated with postsynaptic sites labeled with BTX also appeared to be stably maintained [Fig. 5(A–E), white arrows].

Discussion

BTX Labels Postsynaptic AChRs at an Interneuronal Synapse

Although BTX has been an invaluable tool for visualizing nicotinic AChRs at the vertebrate NMJ, it was somewhat of a surprise that it could be used to image ganglionic synapses via fluorescence microscopy. We found that by adding fluorescently conjugated BTX to the SMGs of living mice, we were able to label AChRs for high-resolution fixed tissue imaging or for vital imaging over time. BTX has previously been used to label ganglionic synapses for electron microscopy (Jacob and Berg, 1983) and to modify their synaptic potentials as monitored by electrophysiology (Marshall, 1981), but relatively few studies have used fluorescent BTX to visualize postsynaptic AChRs on peripheral ganglia and the most successful case is in amphibia (Sargent and Garrett, 1995). Furthermore, to our knowledge, no previous studies have used BTX to visualize postsynaptic AChRs on neurons *in vivo*. Indeed with the exception of the NMJ, this may be the only preparation where neurotransmitter receptors on the postsynaptic membrane can be easily visualized over time.

The BTX labeling suggests that in the submandibular ganglion, postsynaptic AChRs lie in close proximity to all presynaptic terminals. We find that the juxtaposition of pre- and postsynaptic sites remains grossly stable for at least several days. Additionally, since presynaptic stability was similar in BTX labeled and in unlabeled animals [Fig. 3(D) vs. Fig. 5(A–E)], repeated labeling with BTX does not appear to induce changes in synaptic morphology.

Since BTX has been used extensively to characterize the behavior of neuromuscular AChRs, many of those techniques could potentially be applicable to interneuronal synapses. For example, monitoring fluorescence recovery after photobleaching AChR puncta on ganglion cells could be used to measure receptor lateral mobility as it has previously been used on myofibers (Axelrod et al., 1976). Adapting this protocol to neurons would provide insight into the stability of neuronal nicotinic AChRs *in vivo*. It might also be possible to adapt previous methods using BTX (Merlie et al., 1976; Akaaboune et al., 1999) to measure the rates of turnover for neuronal AChRs.

Axo-Somatic Synaptic Connections

In several parts of the nervous system, neurons lack dendrites. In these cases, presynaptic connections sometimes form a basket of processes that surrounds the soma of the postsynaptic cell. The preganglionic innervation to the SMG is one of these cases. Although, in distinction to autonomic ganglia in amphibians (McMahan and Kuffler, 1971), the synapses in the SMG are not axo-somatic *per se*, but rather are located on very fine processes that project a few microns from the cell body and initial segment of the ganglion cell axon (Lichtman, 1977). Similar contacts are also seen on certain CNS neuronal populations including neurons in the auditory system (Schneggenburger and Forsythe, 2006). Interestingly these CNS cells receive convergent innervation from very few neurons, a property they share with SMG cells. The SMG thus appears to be a good model system for certain kinds of central nervous system synaptic connections.

Synaptic Stability and Dynamism

One central question in neurobiology concerns the long-term stability of synaptic connections. This subject has been studied extensively at the neuromuscular junction (Lichtman et al., 1987) and has also been more recently approached in the upper layers of cerebral cortex (Grutzendler et al., 2002; Trachtenberg et al., 2002). The submandibular ganglion is an advantageous preparation for analysis of synaptic dynamism, because unlike other neuronal sites we find it is straightforward to study both pre- and post-synaptic aspects of the same synapses over time. Our initial attempts, described here, suggest that long-term simultaneous pre- and postsynaptic imaging will be possible in this ganglion.

Summary

Technical obstacles associated with *in vivo* visualization of synapses over time have limited the visualization of pre- and postsynaptic sites to relatively few preparations. Therefore, a robust method for imaging interneuronal synapses in living animals should be of broad use to neurobiologists. Studies at the neuromuscular junction have used genetic and pharmacological fluorescent labeling methods to visualize interactions between multiple synaptic elements. Here, we adapt these techniques for imaging synapses in a superficial, accessible part of the parasympathetic nervous system, the mouse SMG. Using laser scanning microscopy, we are able to image these synapses with high spatial resolution (μms) and temporal resolution (from seconds to days) to create four-dimensional data sets to study synapse formation and dynamism. This preparation should be useful for observing and better understanding a range of neurobiological phenomena including naturally occurring synapse elimination, synaptic dynamism, synaptic aging, and synaptic pathology associated with disease; all of which have been shown to take place at SMG synapses (Lichtman, 1977; Gan et al., 2003; Coggan et al., 2004; Yang et al., 2005).

References

Akaaboune M, Culican SM, Turney SG, Lichtman JW. Rapid and reversible effects of activity on acetylcholine receptor density at the neuromuscular junction in vivo. Science 1999;286:503–507. [PubMed: 10521340]

Anderson MJ, Cohen MW. Nerve-induced and spontaneous redistribution of acetylcholine receptors on cultured muscle cells. J Physiol 1977;268:757–773. [PubMed: 69707]

Axelrod D, Ravdin P, Koppel DE, Schlessinger J, Webb WW, Elson EL, Podleski TR. Lateral motion of fluorescently labeled acetylcholine receptors in membranes of developing muscle fibers. Proc Natl Acad Sci USA 1976;73:4594–4598. [PubMed: 1070010]

Balice-Gordon RJ, Lichtman JW. In vivo visualization of the growth of pre- and postsynaptic elements of neuromuscular junctions in the mouse. J Neurosci 1990;10:894–908. [PubMed: 2156964]

Changeux JP, Meunier JC, Huchet M. Studies on the cholinergic receptor protein of *Electrophorus electricus*. I. An assay in vitro for the cholinergic receptor site and solubilization of the receptor protein from electric tissue. Mol Pharmacol 1971;7:538–553. [PubMed: 5139565]

Coggan JS, Grutzendler J, Bishop DL, Cook MR, Gan W, Heym J, Lichtman JW. Age-associated synapse elimination in mouse parasympathetic ganglia. J Neurobiol 2004;60:214–226. [PubMed: 15266652]

Colquhoun LM, Patrick JW. Pharmacology of neuronal nicotinic acetylcholine receptor subtypes. Adv Pharmacol 1997;39:191–220. [PubMed: 9160116]

Feng G, Mellor RH, Bernstein M, Keller-Peck C, Nguyen QT, Wallace M, Nerbonne JM, et al. Imaging neuronal subsets in transgenic mice expressing multiple spectral variants of GFP. Neuron 2000;28:41–51. [PubMed: 11086982]

Fertuck HC, Salpeter MM. Quantitation of junctional and extrajunctional acetylcholine receptors by electron microscope autoradiography after 125I-α-bungarotoxin binding at mouse neuromuscular junctions. J Cell Biol 1976;69:144–158. [PubMed: 1254640]

Gan WB, Kwon E, Feng G, Sanes JR, Lichtman JW. Synaptic dynamism measured over minutes to months: Age-dependent decline in an autonomic ganglion. Nat Neurosci 2003;6:956–960. [PubMed: 12925856]

Gotti C, Clementi F. Neuronal nicotinic receptors: From structure to pathology. Prog Neurobiol 2004;74:363–396. [PubMed: 15649582]

Grutzendler J, Kasthuri N, Gan WB. Long-term dendritic spine stability in the adult cortex. Nature 2002;420:812–816. [PubMed: 12490949]

Jacob MH, Berg DK. The ultrastructural localization of α-bungarotoxin binding sites in relation to synapses on chick ciliary ganglion neurons. J Neurosci 1983;3:260–271. [PubMed: 6822862]

Lee CY, Tseng LF, Chiu TH. Influence of denervation on localization of neurotoxins from clapid venoms in rat diaphragm. Nature 1967;215:1177–1178. [PubMed: 4294063]

Lichtman JW. The reorganization of synaptic connexions in the rat submandibular ganglion during post-natal development. J Physiol 1977;273:155–177. [PubMed: 599418]

Lichtman JW, Magrassi L, Purves D. Visualization of neuromuscular junctions over periods of several months in living mice. J Neurosci 1987;7:1215–1222. [PubMed: 3572477]

Marshall LM. Synaptic localization of α-bungarotoxin binding which blocks nicotinic transmission at frog sympathetic neurons. Proc Natl Acad Sci USA 1981;78:1948–1952. [PubMed: 6972045]

McCann CM, Bareyre FM, Lichtman JW, Sanes JR. Peptide tags for labeling membrane proteins in live cells with multiple fluorophores. Biotechniques 2005;38:945–952. [PubMed: 16018556]

McCann CM, Bracamontes J, Steinbach JH, Sanes JR. The cholinergic antagonist α-bungarotoxin also binds and blocks a subset of GABA receptors. Proc Natl Acad Sci USA 2006;103:5149–5154. [PubMed: 16549768]

McMahan UJ, Kuffler SW. Visual identification of synaptic boutons on living ganglion cells and of varicosities in postganglionic axons in the heart of the frog. Proc R Soc Lond B Biol Sci 1971;177:485–508. [PubMed: 4396517]

Merlie JP, Changeux JP, Gros F. Acetylcholine receptor degradation measured by pulse chase labelling. Nature 1976;264:74–76. [PubMed: 1004540]

Nguyen QT, Sanes JR, Lichtman JW. Pre-existing pathways promote precise projection patterns. Nat Neurosci 2002;5:861–867. [PubMed: 12172551]

Orr-Urtreger A, Goldner FM, Saeki M, Lorenzo I, Goldberg L, De Biasi M, Dani JA, et al. Mice deficient in the α7 neuronal nicotinic acetylcholine receptor lack α-bungarotoxin binding sites and hippocampal fast nicotinic currents. J Neurosci 1997;17:9165–9171. [PubMed: 9364063]

Purves D, Lichtman JW. Synaptic sites on reinnervated nerve cells visualized at two different times in living mice. J Neurosci 1987;7:1492–1497. [PubMed: 3572488]

Sanes JR, Lichtman JW. Induction, assembly, maturation and maintenance of a postsynaptic apparatus. Nat Rev Neurosci 2001;2:791–805. [PubMed: 11715056]

Sargent PB, Garrett EN. The characterization of α-bungarotoxin receptors on the surface of parasympathetic neurons in the frog heart. Brain Res 1995;680:99–107. [PubMed: 7663990]

Schneggenburger R, Forsythe ID. The calyx of Held. Cell Tissue Res 2006;326:311–337. [PubMed: 16896951]

Sekine-Aizawa Y, Huganir RL. Imaging of receptor trafficking by using α-bungarotoxin-binding-site-tagged receptors. Proc Natl Acad Sci USA 2004;101:17114–17119. [PubMed: 15563595]

Snider WD. The dendritic complexity and innervation of submandibular neurons in five species of mammals. J Neurosci 1987;7:1760–1768. [PubMed: 3598646]

Trachtenberg JT, Chen BE, Knott GW, Feng G, Sanes JR, Welker E, Svoboda K. Long-term in vivo imaging of experience-dependent synaptic plasticity in adult cortex. Nature 2002;420:788–794. [PubMed: 12490942]

Walsh MK, Lichtman JW. In vivo time-lapse imaging of synaptic takeover associated with naturally occurring synapse elimination. Neuron 2003;37:67–73. [PubMed: 12526773]

Ward JM, Cockcroft VB, Lunt GG, Smillie FS, Wonnacott S. Methyllycaconitine: A selective probe for neuronal α-bungarotoxin binding sites. FEBS Lett 1990;270:45–48. [PubMed: 2226787]

Yang G, Gong YD, Gong K, Jiang WL, Kwon E, Wang P, Zheng H, et al. Reduced synaptic vesicle density and active zone size in mice lacking amyloid precursor protein (APP) and APP-like protein 2. Neurosci Lett 2005;384:66–71. [PubMed: 15919150]

Zarei MM, Radcliffe KA, Chen D, Patrick JW, Dani JA. Distributions of nicotinic acetylcholine receptor α7 and β2 subunits on cultured hippocampal neurons. Neuroscience 1999;88:755–764. [PubMed: 10363815]

Zuo Y, Lubischer JL, Kang H, Tian L, Mikesh M, Marks A, Scofield VL, et al. Fluorescent proteins expressed in mouse transgenic lines mark subsets of glia, neurons, macrophages, and dendritic cells for vital examination. J Neurosci 2004;24:10999–11009. [PubMed: 15590915]

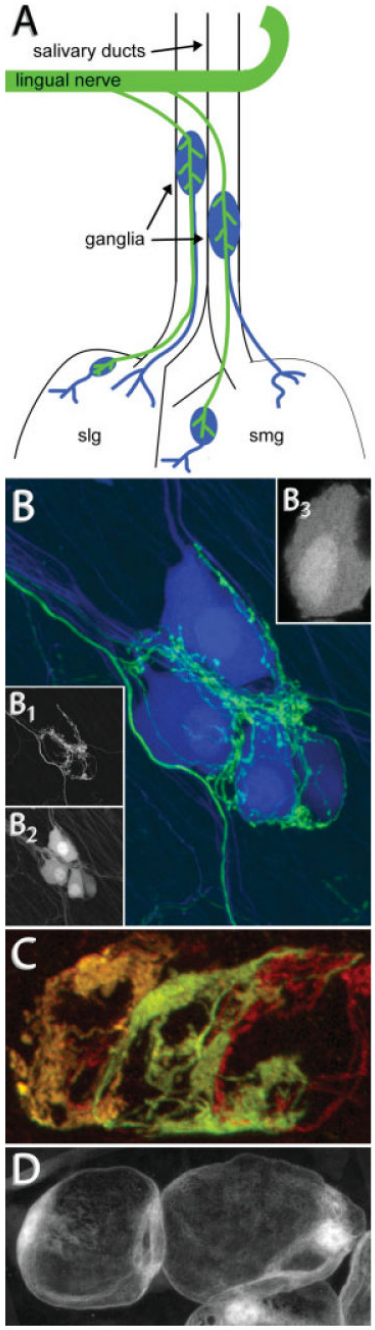

Figure 1.
Vital labeling of synapses in the adult mouse SMG. (A) Preganglionic axons (green) project from the superior salivatory nucleus in the brain stem to the lingual nerve where they branch to innervate several groups of postganglionic neurons (blue). Postganglionic neurons send fasciculated axons into the submandibular (smg) and sublingual (slg) salivary glands where they innervate myoepithelial cells in the gland parenchyma. Ganglia located on the salivary ducts can be easily accessed *in vivo*. (B) Confocal stack taken from a thy1-double transgenic animal expressing YFP in preganglionic neurons (green) and CFP in postganglionic neurons (blue). (B_1) Preganglionic axons form basket-like structures where they synapse onto postganglionic neurons. (B_2) Postganglionic neurons lack long dendrites and receive inputs

onto pseudodendrites on their soma. They project axons to innervate cells in the salivary gland. (B_3) The surface of fluorescently labeled ganglion cells is rough, reflecting the presence of pseudodendrites. (C) Confocal stack taken from a double transgenic animal expressing CFP (red) and YFP (green) in overlapping subsets of preganglionic neurons. Shown is the preganglionic innervation to three postganglionic neurons. The ratio of CFP:YFP is different in each axon, allowing for the discrimination of three separate axons (orange, yellow, and red). (D) Confocal stack taken from an animal expressing GFP in Schwann cells. Schwann cells surround postganglionic neurons to envelop preganglionic connections.

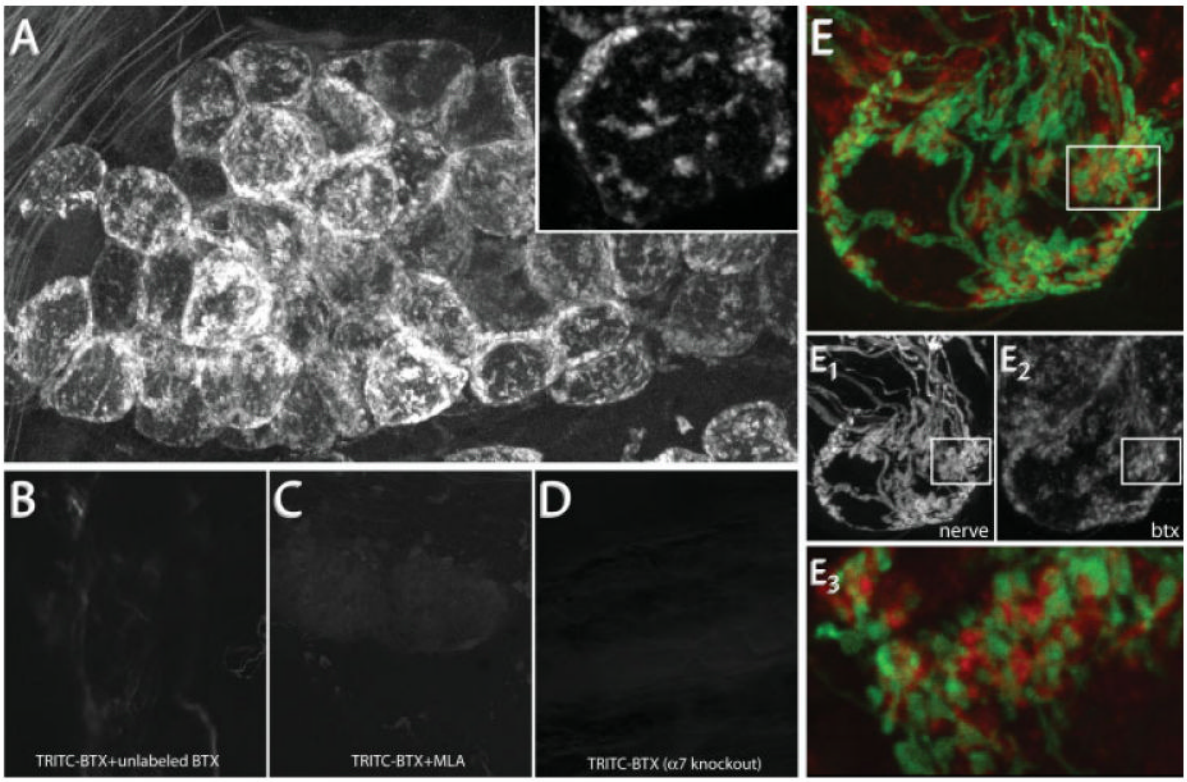

Figure 2.

BTX specifically labels postsynaptic AChR α7. (A) BTX labeling in the SMG. 10 n*M* TRITC-BTX was added to the neck of an anesthetized wild-type mouse. After BTX labeling (1 h), postganglionic neurons display punctate fluorescent labeling. Inset shows clusters of fluorescence on the surface of two postganglionic neurons. (B) Pre- and coincubation with a saturating dose of unlabeled BTX blocks TRITC-BTX labeling. (C) Methyllycaconitine (MLA), a reagent known to specifically block the interaction between BTX and AChR α7, blocks TRITC-BTX labeling in SMG. (D) BTX labeling is not present in the SMG of genetically modified animals (red) lacking the AChR α7 subunit. Image acquisition parameters were the same for (A) through (D). (E) BTX labeling (red) is selectively opposed to presynaptic terminals (green). ($E_{1,2}$) Single channel images from (E) depicting YFP labeled preganglionic axons (E_1) and BTX labeled postsynaptic AChRs (E_2). (E_3) Single optical section of the boxed region in (E) shows that YFP-labeled presynaptic terminals are closely juxtaposed to BTX labeled regions.

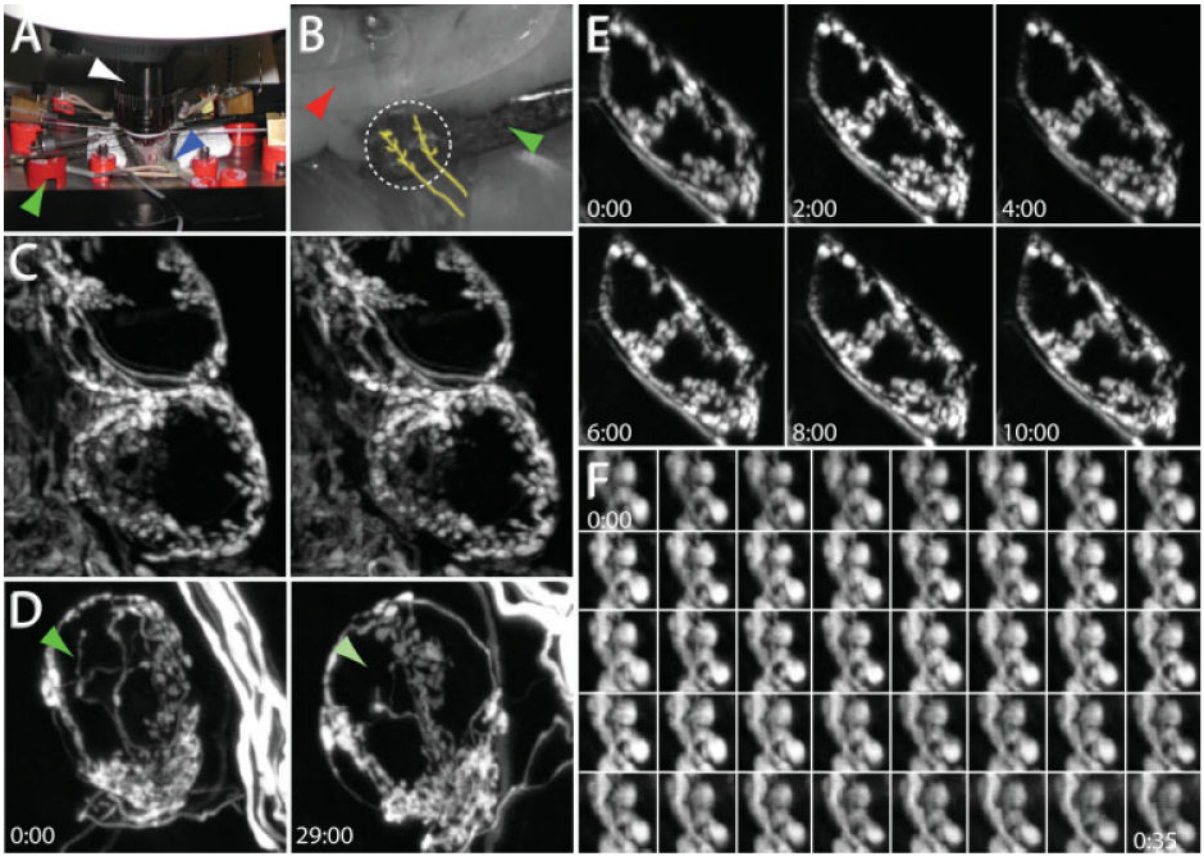

Figure 3.

In vivo time-lapse imaging in the SMG. (A) *In vivo* imaging setup. A 60× water immersion objective (white arrow) is placed into a cavity created by a ventral midline neck incision in an anesthetized and mechanically ventilated mouse. The blue arrow indicates the endotracheal tube connected to a small animal ventilator, and the green arrow indicates one of the retractors used to maintain the opening at the site of the neck incision. (B) The salivary ducts are placed on retractors to provide stability. One retractor (green arrow) is placed below the salivary ducts while a second retractor (red arrow) is placed on top of the submandibular gland. The location of the preganglionic axon bundles are roughly traced in yellow. The region to be imaged is indicated by the dashed white circle. (C) Stereo-pair images from an image stack depicting the preganglionic innervation to several postganglionic neurons. (D) Presynaptic axons can be visualized over days. After taking the image on the left, the neck wound was sutured closed and the animal was returned to the cage and allowed to recover. Twenty-nine hours later, the animal was reanesthetized and the same structures relocated. The green arrow indicates the location of a presynaptic terminal that was present at the beginning of the imaging session but absent the next day. (E) Presynaptic axons can be visualized chronically over hours. YFP-labeled preganglionic axons were stable when imaged every 2 h for 10 h. (D, E) Times indicate hours:minutes. (F) Presynaptic boutons imaged every minute for 35 min. Times represent minutes:seconds.

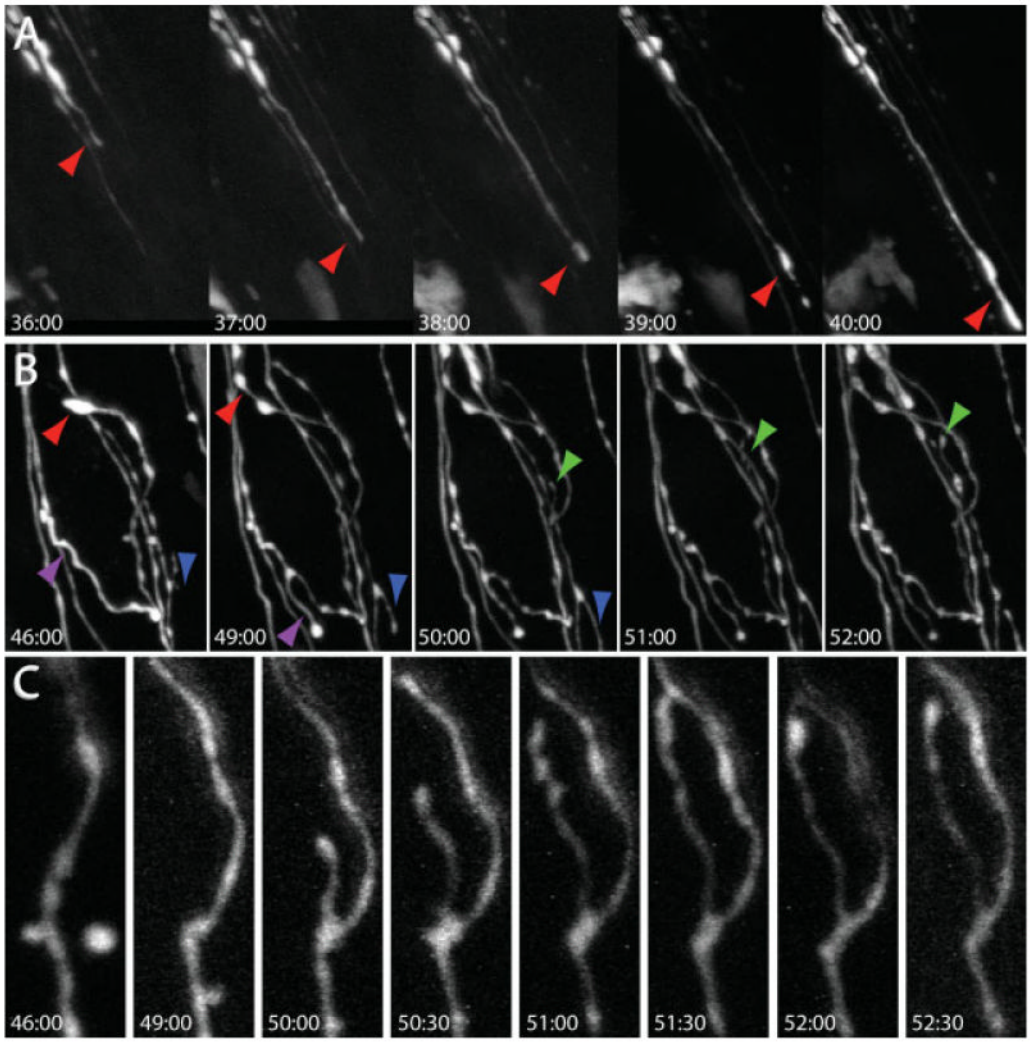

Figure 4.

In vivo time-lapse imaging of axon growth and synapse formation. Preganglionic axons were crushed with a blunt forceps along the salivary ducts at time 0:00 and imaged at the indicated times after crush (hr:min). (A) 1 [1/2] days later, regrowth could be observed as preganglionic axons grew toward postganglionic neurons. Red arrows indicate sites of axon advance. (B) Axons rapidly reinnervate postsynaptic postganglionic neurons (dark region in the middle of the image) by sending processes that wrap around the soma. Colored arrows indicate sites of axon elongation. (C) When preganglionic axons contact postganglionic neurons, presynaptic boutons appear along axonal branches as axons change from a uniform to a scalloped shape.

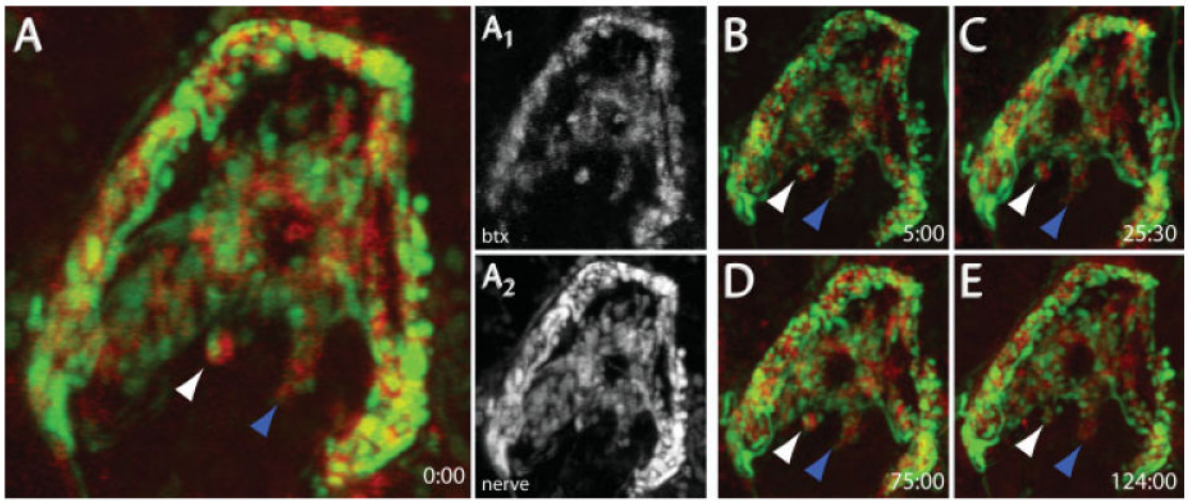

Figure 5.

In vivo time-lapse imaging of pre- and postsynaptic structures. YFP-labeled presynaptic axons and BTX-labeled AChRs were imaged over time. 647-BTX was added to the neck for 1 h, and then washed out with Ringer's solution. YFP-labeled preganglionic axons (A_2) and 647-BTX-labeled postsynaptic AChRs (A_1) were simultaneously imaged on a confocal microscope. (B–E) After the first image, the wound was sutured closed and the animal was allowed to recover. Synapses were relabeled with BTX for each successive imaging session. Arrows indicate individual synaptic regions that could be identified for several days. The white arrow indicates stable presynaptic terminals and postsynaptic AChRs, while the blue arrow shows a region where presynaptic terminals are dynamic but postsynaptic AChRs are stable. Times correspond to hr:min.